

High Voltage CMOS Control Interface for Astronomy - Grade Charged Coupled Devices

Elena Martin^{a,*}, Gary Varner^a, Aaron Koga^a, Larry Ruckman^a, Peter Onaka^b, John Tonry^b, and Aaron Lee^b

^a

*Department of Physics and Astronomy,
University of Hawaii, 2505 Correa Rd., Honolulu, Hawaii, 96822, USA*

^b *Institute for Astronomy,*

*University of Hawaii, Honolulu, 2680 Woodlawn Drive, Hawaii, 96822, USA
E-mail: elena.martin@cnm.es*

ABSTRACT: The Pan-STARRS telescope consists of an array of smaller mirrors viewed by a Giga-pixel arrays of CCDs. These focal planes employ Orthogonal Transfer CCDs (OTCCDs) to allow on-chip image stabilization. Each OTCCD has advanced logic features that are controlled externally. A CMOS Interface Device for High Voltage has been developed to provide the appropriate voltage signal levels from a readout and control system designated STARGRASP. OTCCD chip output levels range from -3.3V to 16.7V, with two different output drive strengths required depending on load capacitance (50pF and 1000pF), with 24mA of drive and a rise time on the order of 100ns. Additional testing Wilkinson ADC structures have been included in this chip to evaluate future functional additions for a next version of the chip.

KEYWORDS: OTCCD; CCD; High Voltage CMOS; telescope.

*Corresponding author.

Contents

1. Introduction	1
2. CID Background	2
3. CID High Voltage Chip	3
3.1 Level Shifting Signal Subsection	5
3.1.1 Architecture used for the Level Shift Subsection	6
3.1.2 Waveforms obtained	6
3.1.3 Rise and Fall Time Measurements	7
3.2 Testing Structures	8
3.2.1 ADC Ramp circuit	8
3.2.2 ADC Comparator Testing	9
3.2.3 Sample and Hold Testing	9
4. Conclusion	10

1. Introduction

The Panoramic Survey Telescope and Rapid Response System (Pan-STARRS) is an innovative design for a wide-field imaging facility being developed at the University of Hawaii's Institute for Astronomy. The combination of small mirrors with very large digital cameras allows the development and deployment of an economical observing system that will be able to survey the entire available sky several times each month.

The immediate goal of Pan-STARRS is to discover and characterize Earth-approaching objects, both asteroids and comets, that might pose a danger to our planet. The design of Pan-STARRS is heavily weighted towards its primary purpose, which is to detect potentially hazardous objects in the Solar System. But the wide-field, repetitive nature of the Pan-STARRS observations makes them ideal for a host of other astronomical purposes, ranging from Solar System astronomy to cosmology. There are two features that distinguish Pan-STARRS from other astronomical surveys: its ability to map very large areas of sky with great sensitivity and its ability to find moving or variable objects.

Pan-STARRS will eventually consist of four individual optical systems, each with a 1.8 meter diameter mirror observing the same region of sky simultaneously. Each mirror will have a 3 degree field of view and be equipped with a digital CCD camera containing 1.4 billion pixels. The spatial sampling of the sky will be about 0.3 arcseconds. While searching for potential killer asteroids in

survey mode, Pan-STARRS will cover $6,000 \text{ deg}^2$ per night. The whole available sky as seen from Hawaii will be observed 3 times during the dark time in each lunar cycle. The focal planes will employ **Orthogonal Transfer CCDs (OTCCDs)** that feature on-chip image motion compensation.

To evaluate many of the features of the full telescope, a prototype system designated PS1 has been developed. PS1 is essentially one quarter of Pan-STARRS. It has the same optics and camera design as proposed for the full version of Pan-STARRS. PS1 has been built on the site of the south dome of the old LURE observatory on Haleakala, Maui. First light occurred in June 2006 and the telescope was formally dedicated on June 30, 2006. The first of the Gigapixel cameras was installed in August 2007. PS1 serves to test all the technology that is being developed for Pan-STARRS, including the telescope design, the cameras, and the data reduction software. PS1 will be used to make a full-sky survey that will provide astrometric and photometric calibration data that will be used for the full Pan-STARRS survey.

An overview of the OTA used in the Pan-STARRS project is found in Section 2. Section 3 introduces the High Voltage control chip that has been developed. This chip has two main structures. The first structure contains the Level Shifting circuitry, described in Subsection 3.1, where test results are presented. The second structure is a set of Test circuits, which are described in Subsection 3.2, and where test results for the ADC are presented.

2. CID Background

The Orthogonal-Transfer Array (OTA) is a CCD architecture designed to provide wide-field tip-tilt correction of astronomical images. This device consists of an 8×8 array of small orthogonal-transfer CCDs (OTCCD) with independent addressing and readout of each OTCCD. This approach enables an optimum tip-tilt correction to be applied independently to each OTCCD across the focal plane. This device was developed by MIT Lincoln Laboratory in support of the Pan-STARRS program (see [8] and [9] for more details) collaborative effort with Semiconductor Technology Associates (STA) for the WIYN Observatory.

A small, evaluation version of the OTA is called a mini-OTA (MOTA) and consists of a 2×2 arrays of OTCCD cells, shown schematically in Figure 1. This MOTA was included in the wafer layout and has advanced control features of future interest. Inclusion of MOTA structures allows the novel nature of the OTCCD devices to be explored while respecting the compressed schedule for device deliveries [6], [7].

MOTAs provide the opportunity to try advanced features, such as two-phase serial registers, dual output gates and higher performance designs. Each cell has an associated control-logic block, as shown in Fig. 2. The logic block accepts 3 data bits (D2-D1-D0) as inputs and outputs 3 logic levels (Z2-Z1-Z0) to control the parallel clock waveforms applied to each cell (with Z0 and Z1) and to gate the output of the amplifier onto the video column bus OUTn (with signal Z2). The parallel clock voltages applied to each cell are set by four active clock levels, P1A-P4A, and to standby voltages, PSH and PSL, all from off-chip circuitry.

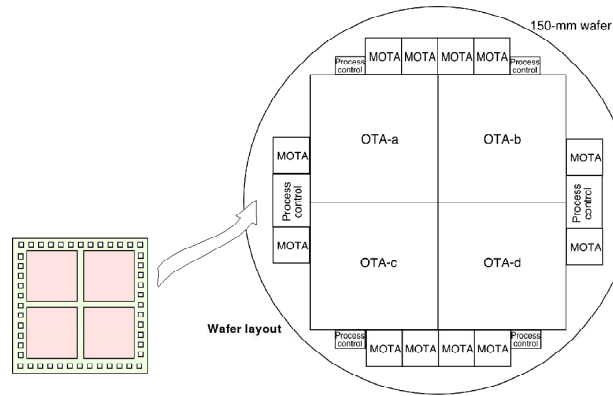


Figure 1. Basic Mini-OTA locations on wafer.

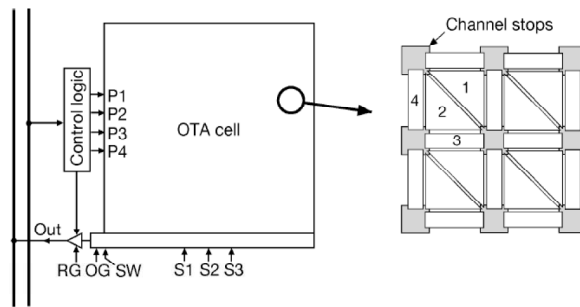


Figure 2. Basic architecture for the OTA cell.

3. CID High Voltage Chip

The CMOS Interface Device for High Voltage version 0 (CID0) is a microelectronic chip that has been developed using the $0.35\mu\text{m}$ High Voltage process from AustriaMicroSystems. The main purpose of this chip is to provide the appropriate voltage signal levels from the STARGRASP¹ [5] readout and control system to the MOTA chip [2, 3, 4]. CID0 also has additional signals for output monitoring. Some additional test structures have been included in order to evaluate future additions for a next version of the chip.

The main structures of this chip are visible in Fig. 3. Table 1 lists the input and output signals and Table 2 the voltage level requirements. The external layout dimensions are $3262 \times 3218 \mu\text{m}$ (see Fig. 4 to see a photograph of the chip at the package). Minimum pad pitch is $123\mu\text{m}$.

¹<http://www.stargrasp.org/>

Table 1. Voltage levels for the MOTA chip

Output	Pin Name	V _{DD}	V _{SS}	Ref. Level	Ref. Level
1	RSEL1	V _{DD_HV1}	V _{SS_HV1}	VDDL	LREF
2	RSEL0	V _{DD_HV1}	V _{SS_HV1}	VDDL	LREF
3	SW	V _{DD_HV2}	V _{SS_HV2}	VDDS	LREF
4	S3	V _{DD_HV2}	V _{SS_HV2}	VDDS	LREF
5	S2	V _{DD_HV2}	V _{SS_HV2}	VDDS	LREF
6	S1	V _{DD_HV2}	V _{SS_HV2}	VDDS	LREF
7	P4A	V _{DD_HV3}	V _{SS_HV3}	VDDH	LREF
8	P3A	V _{DD_HV3}	V _{SS_HV3}	VDDH	LREF
9	P2A	V _{DD_HV3}	V _{SS_HV3}	VDDH	LREF
10	P1A	V _{DD_HV3}	V _{SS_HV3}	VDDH	LREF
11	PSH	V _{DD_HV3}	V _{SS_HV3}	VDDH	LREF
12	PSL	V _{DD_HV3}	V _{SS_HV3}	VDDH	LREF
13	RG	V _{DD_HV4}	V _{SS_HV4}	VDDG	LREF
14	CSEL1	V _{DD_HV1}	V _{SS_HV1}	VDDL	LREF
15	D2	V _{DD_HV1}	V _{SS_HV1}	VDDL	LREF
16	D1	V _{DD_HV1}	V _{SS_HV1}	VDDL	LREF
17	D0	V _{DD_HV1}	V _{SS_HV1}	VDDL	LREF
18	CSEL4	V _{DD_HV1}	V _{SS_HV1}	VDDL	LREF

Table 2. Voltage Levels correspondence for Table 1.

# Pins			Typ.(V)	Min.(V)	Max.(V)
2	VDD	3.3	3.3		4
2	VSS	0	0	-0.4	
2	VDD_HV1	LREF+7	5		8
2	VSS_HV1	LREF	-2	-10	
2	VDD_HV2	10	5		16
2	VSS_HV2	-6	-3	-10	
2	VDD_HV3	LREF+9	7		15
2	VSS_HV3	LREF+1	-1	-10	
2	VDD_HV4	10	5		16
2	VSS_HV4	-5	-3	-10	

Three main circuit elements included in CID0 occupy different areas of the floorplan and use the following areas: the **Level Shifting Subsection** of $1390 \times 1470 \mu m$ for the high current drive circuit and $432 \times 940 \mu m$ for the low current drive circuit, **Monitor Output Signals** area of $945 \times 755 \mu m$ and **Testing Structures** is $1020 \times 2050 \mu m$.

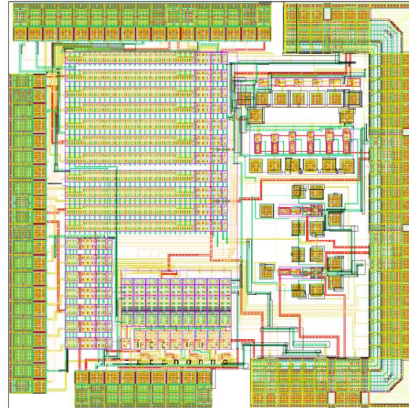


Figure 3. Cadence Layout for the High Voltage Chip.

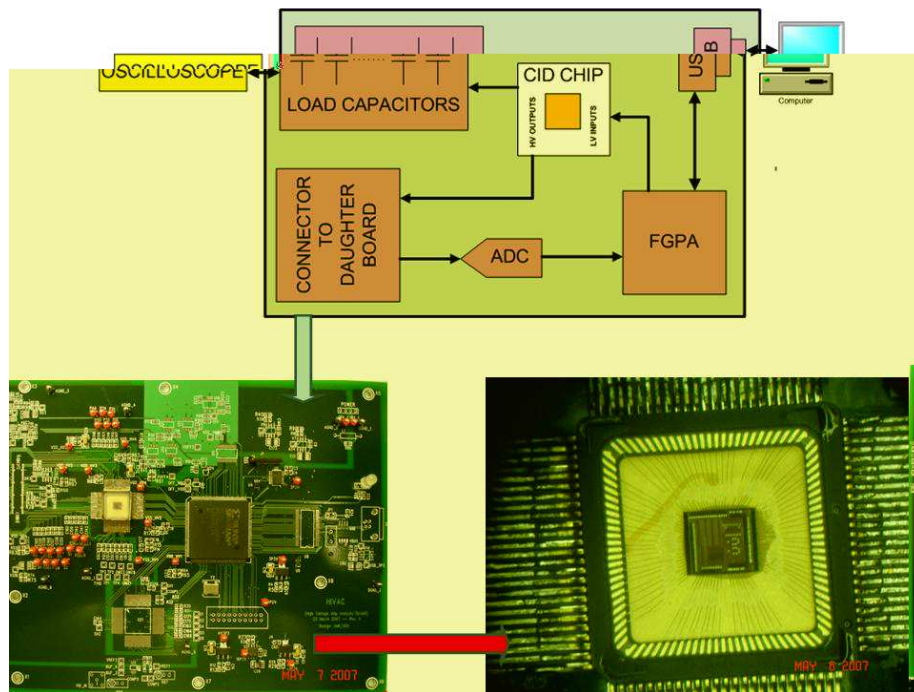


Figure 4. Top image shows the general schematic of the system developed to use the High Voltage Chip, the connector to the daughter board correspond to the CCD connector. The bottom left image shows a photograph of the real board, where the chip can be observed on the left top side of the image. The bottom right image shows a photograph of the chip, where all the wire bondings done (with lengths of $\sim 3\text{mm}$ have been used) can be observed.

3.1 Level Shifting Signal Subsection

The level shifting circuitry occupies most of the layout. In all cases, the input signal is a digital signal with input voltage levels from 0-3.3V. The output signal corresponds to the input, but with

shifted levels and increased drive strength. There are 2 different capacitive load configurations, 50pF and 1000pF, and in both cases the circuit has to be able to drive up to 25mA. For either case, the rise time is required to be 100ns.

A 3-stage topology has been adopted: a pre-amplifier that takes the signals from an initial 0-3.3V and translates to -3.3V to 16.7V, and a 2-stage output buffer, as indicated in Fig. 5. In both cases (high or low load capacitance) the pre-amplifier and the 1st level output buffer are equal. The 2nd level buffer determines the final strength of the signal. The voltage levels to which the various outputs are set are summarized in Table 1 and Table 2.

3.1.1 Architecture used for the Level Shift Subsection

The architecture developed for the Level Shift Subsection consists of 3 different parts, as seen in Fig. 5.

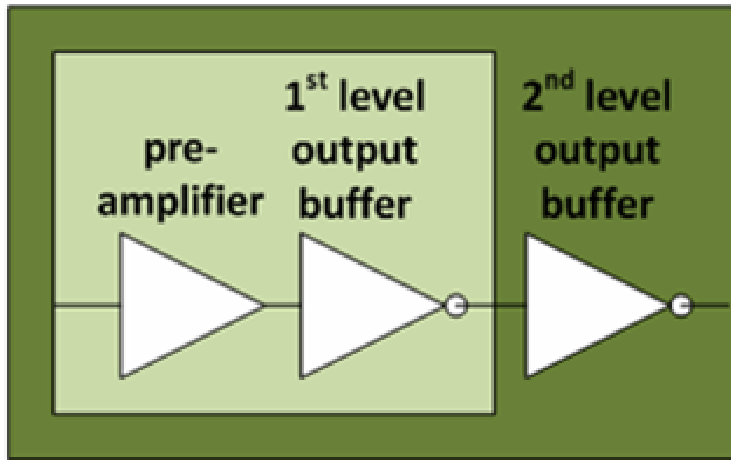


Figure 5. General diagram of the Level Shift circuitry.

The pre-amplifier and the 1st level buffer convert the signal to the voltage levels needed at every Voltage Output rail. The pre-amplifier is a basic input-differential comparator that converts a low-voltage TTL signal to the extended maximum level (-3.3V, 16.7V). The 1st level buffer shrinks the signal as defined in Table 2, and uses a group of 3 inverters that are used as buffers. The size of these transistors are small, using $(w/l)_p=40/5$ and $(w/l)_n=40/2.5$. The third and last stage is a 2nd level buffer, which determines the final strength of the output signal drive. It consists of 1 inverter, with 2 different w/l sizes, depending on the required output drive strength needed. For loads of 50pF a $(w/l) = 200/3$ is used, and for loads of 1000pF a $(w/l) = 2240/3$ is used.

3.1.2 Waveforms obtained

The output waveforms observed in the measurements show ringing coming from the bonding wire inductance. Fig. 6 is a sample Output Voltage for the HV2 rail case. This signal (S1) is driving a load capacitance of 300pF. Fig. 7 correspond to another example of the ringing observed for the

RG signal in the case the output voltage is at HV4 levels and a load capacitor with value of 51pF is used.

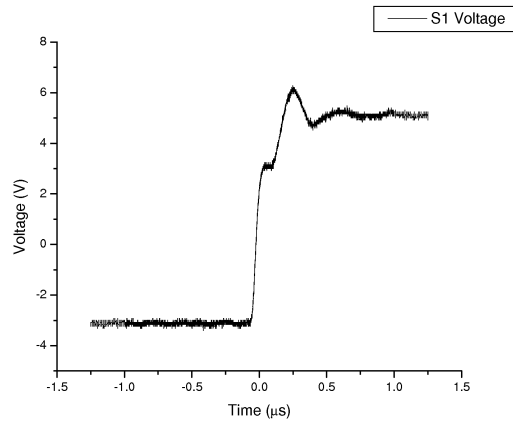


Figure 6. S1 Output voltage signal for a 300pF load capacitance.

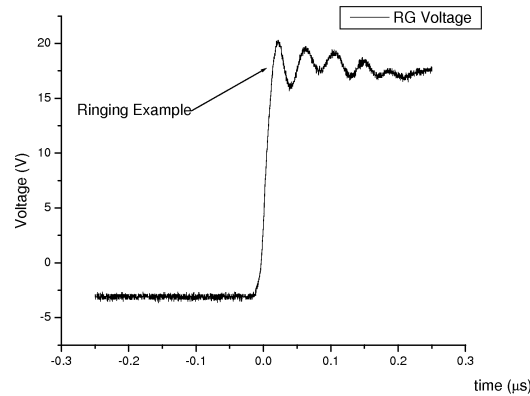


Figure 7. RG Ringing Output Voltage for a 51pF load.

3.1.3 Rise and Fall Time Measurements

Rise and Fall time measurements have been performed for voltages HV1-HV4, and these transition times are shown in Fig. 8-11, respectively. These figures show the results of the transition times observed for a specific range of load capacitances, corresponding to the expected MOTA load condition for those signal lines.

Expected load values for signals of the HV1 are 50pF. The rise and fall times are slightly larger than expected, with rise times that are $\sim 180ns$ for the expected output load capacitance. Typical capacitance load values for output banks HV2, HV3 and HV4 are 1000pF. The measurements are again longer and higher than had been hoped. The primary reason is that the maximum drive strength obtained for the pads in this process corresponds to only 24 mA. This value gives a

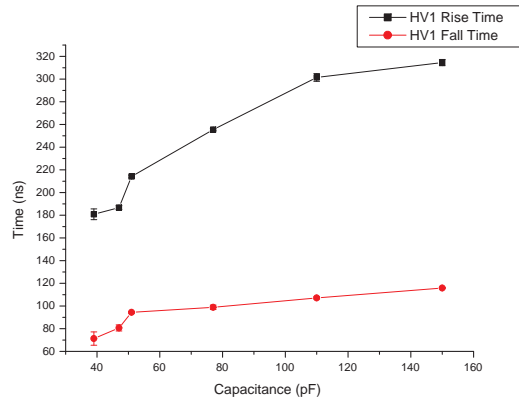


Figure 8. HV1 rise and fall time measurements versus capacitive load.

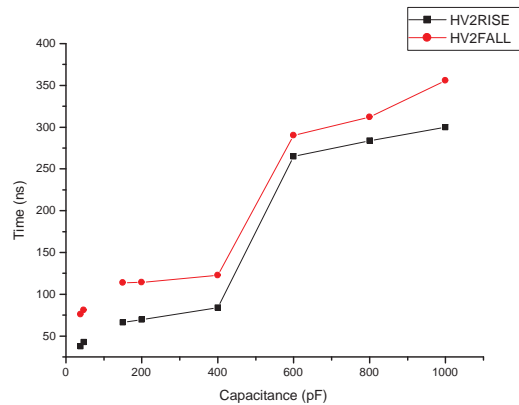


Figure 9. HV2 rise and fall time measurements versus capacitive load.

theoretical rise/fall time value for the 1000pF load that is about 3 times the desired value (100ns). The highest values found in Fig. 8 are 300ns for the rise time and 350ns for the fall time.

3.2 Testing Structures

To evaluate future architectures for inclusion of a possible ADC in the next CID version, 3 different testing structures have been included in this chip.

3.2.1 ADC Ramp circuit

The simple structure shown in Figure 12 has been included, where six different values for the capacitors have been used (from 0.80pF to 3.12pF). The capacitor used is C_{poly} , formed from poly1 and poly2.

In all configurations the C_{ramp} gets dominated by oscilloscope capacitance (12pF), with $\Delta V=3.3V$ and $\Delta t=2.8ms$, showing the current is higher than initially simulated (2.55mA vs 1.0mA)

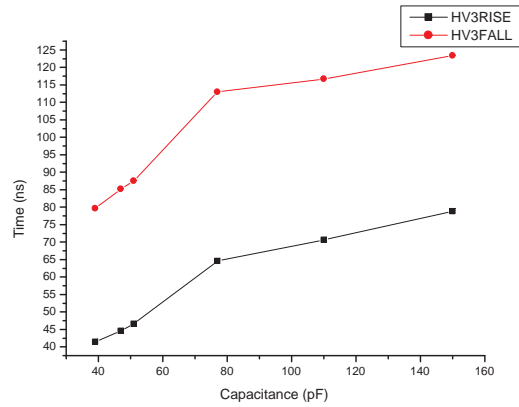


Figure 10. HV3 rise and fall time measurements versus capacitive load.

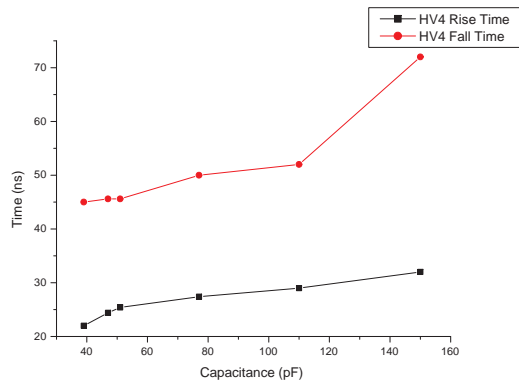


Figure 11. HV4 rise and fall time measurements versus capacitive load.

3.2.2 ADC Comparator Testing

This structure includes the previous structure and a comparator. The comparator is a voltage comparator with a preamplification stage, a decision circuit stage and an output buffer that works at 1MHz. Fig. 13 shows a general schematic that includes the ramp generator that is also present in this configuration.

3.2.3 Sample and Hold Testing

In this structure a differential storage of the value is done and then shifted using a reference value. This value is then used for the comparison with the ramp signal, the comparator output of which time encodes the analog value. Fig. 14 illustrates the general architecture. To test this structure, an FPGA-based TDC has been used [1], with a 2ns time step and a measured time resolution of 0.604ns, as plotted in Fig. 15. The measured transfer curve is displayed in Fig. 16. Noise coming

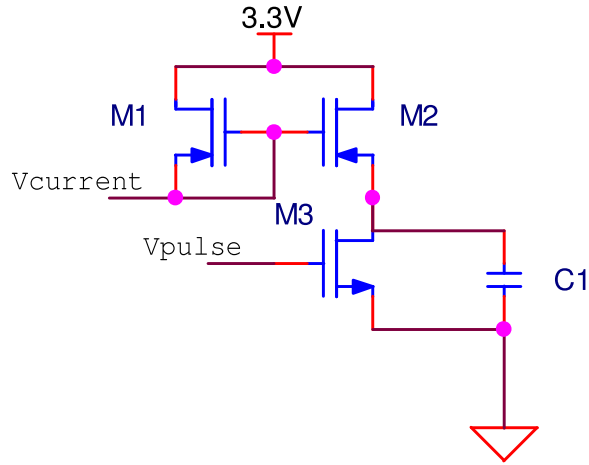


Figure 12. Cadence Schematic for the Ramp Generator.

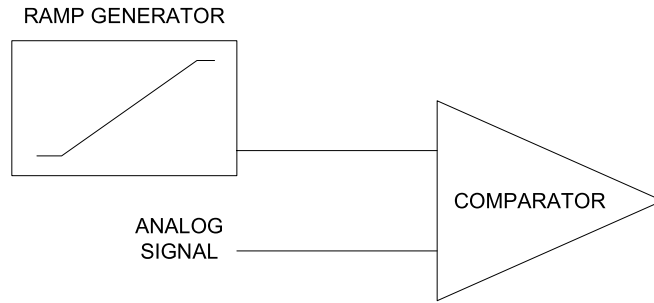


Figure 13. General architecture for the ADC Comparator structure.

from the jitter of the FPGA has been subtracted from the total RMS noise, see Fig. 17, according to Eq. 3.1. Fig. 18 shows the residual errors obtained in the voltage determination.

$$\sigma_{measure}^2 = \sigma_{edges}^2 + \sigma_{FPGA}^2 \quad (3.1)$$

A fitting of the distribution has been done using a second order polynomial, with $Time = A + B1 \times Vref + B2 \times Vref^2$, with weights given by the error bars. The fitting parameters obtained are $A = 160.75 \pm 40.56$ ns, $B1 = -38.78 \pm 45.45$ ns/V, $B2 = 163.83 \pm 11.95$ ns/V². The correlation coefficient value is $r=0.9955$, which promises good performance of the system.

4. Conclusion

MOTA CCDs need control signal levels that are much different than those typically available for standard logic and need to span something like -5V to 20V. To provide this level translation the

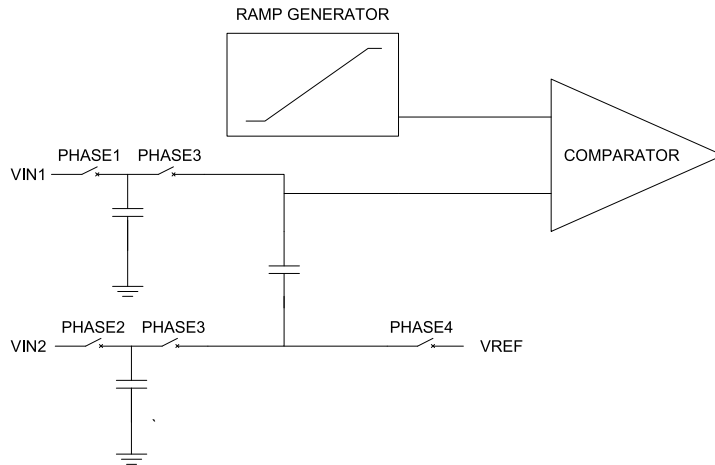


Figure 14. Sample and Hold general architecture.

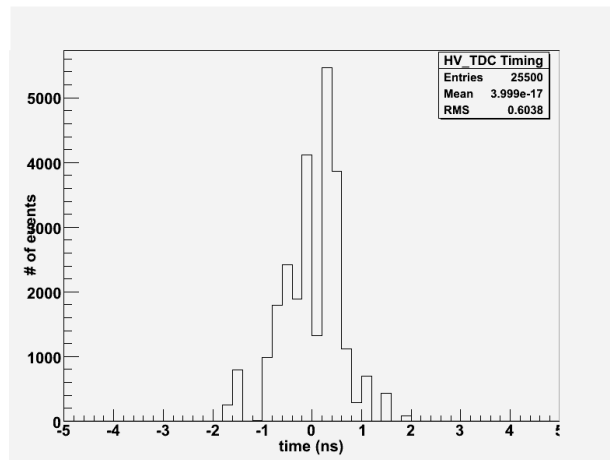


Figure 15. Measurement of the TDC time resolution.

CID0 HV CMOS ASIC has been fabricated and tested. This chip has been used to evaluate the $0.35\mu\text{m}$ HV process from AustriaMicrosystems. The CID0 chip includes the level shifting circuitry needed for MOTA interfacing, as well as some additional testing structures. The High Voltage Chip is interfaced to the CCD using a Flex connector during the test of the prototype. The final goal of this project is to integrate in the same substrate the CCD and the chip, this approach will also prevent any more ringing problems coming from the inductance at the bonding wires used in this version. Observed level shift circuitry performance matches expectations for this process, although the drive strength of the pads used here is not sufficient for a final 10MHz operation. In order to meet the design requirements there is an option that has been analyzed. This option is to develop our own pads, which will show a suitable drive strength value, for the time being the CID0 chip will be used with the actual performance. Wilkinson ADC test structures have been evaluated and show promise for implementing complex readout structures in close proximity and at the high voltage levels typical of OTCCD devices.

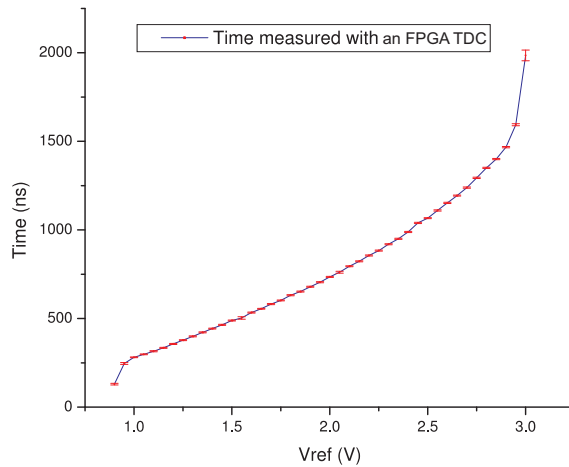


Figure 16. Results for the Wilkinson ADC conversion.

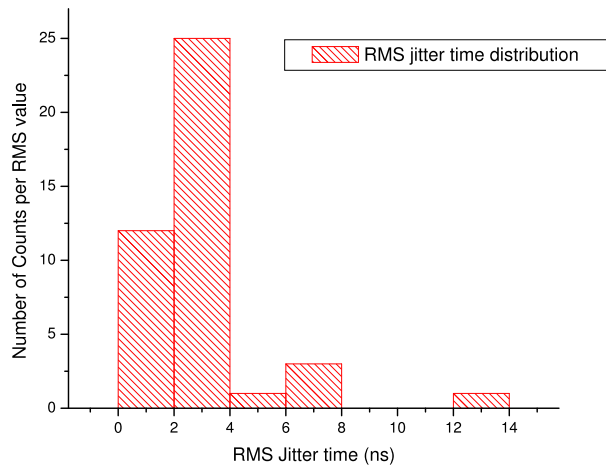


Figure 17. Distribution of RMS noise.

Acknowledgments

The authors thank the Vice Chancellor for Research of the University of Hawaii for his support of this project.

References

- [1] G. Varner, *The Modern FPGA as Discriminator, TDC and ADC*, 2006 *JINST* **1** P07001.
- [2] B. Burke, *An Orthogonal-Transfer CCD Imager*, *Rev. IEEE Trans. Elec. Dev.*, **41** (1994) 12 2482-2484.
- [3] D. Smith *et al*, *Development and Testing of a 2-D Transfer CCD*, *IEEE Trans. Elec. Dev.*, **53** (2006) 11 (2748-2754).
- [4] S. Howell *et al*, *Photometric Observations Using Orthogonal Transfer CCDs*, *Publications of the Astronomical Society of the Pacific*, **115** (2003) 1340-1350.

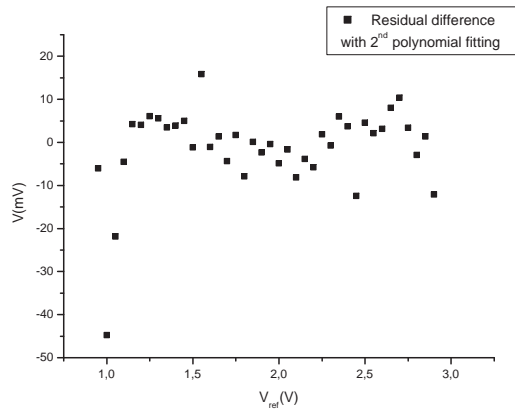


Figure 18. Residual errors in the voltage determination.

- [5] S. Keller *et al*, *The SkyMapper Telescope and The Southern Sky Survey*, *Publications of the Astronomical Society of Australia*, **24** (2007) 1-12.
- [6] B. Burke *et al*, *Development of the orthogonal-transfer array*, in *Sensors, Cameras and Systems for Scientific/Industrial Applications VII*, 173-180, SPIE, 2006.
- [7] B. Burke *et al*, *The orthogonal-transfer array: a new CCD architecture for astronomy*, in *Optical and Infrared Detectors for Astronomy*, 185-192, SPIE, 2004
- [8] K. Hodapp, *Design of the Pan-STARRS telescopes*, *Astron. Nachr.*, **325** (2004) 636-642.
- [9] N. Kaiser, *Pan-STARRS: a wide-field optical survey telescope array*, *Proceedings of SPIE - Ground-based Telescopes*, **5489** (2004) 11-22.